Proceedings of the ASME 2018 International Mechanical Engineering Congress and Exposition
IMECE2018
November 9-15, 2018, Pittsburgh, PA, USA

IMECE2018-86947

MULTISCALE INVESTIGATION OF THICKNESS DEPENDENT MELTING THRESHOLDS OF NICKEL FILM UNDER FEMTOSECOND LASER HEATING

Pengfei Ji, Mengzhe He and **Yiming Rong**
Shenzhen Key Laboratory for Additive Manufacturing of High-performance Materials
Department of Mechanical and Energy Engineering
Southern University of Science and Technology
Shenzhen 518055, China
E-mail: pengfeiji2htec@outlook.com

Yuwen Zhang
Department of Mechanical and Aerospace Engineering
University of Missouri
Columbia MO 65211, USA

Yong Tang
Key Laboratory of Surface Functional Structure Manufacturing of Guang Dong Higher Education Institutes
School of Mechanical and Automotive Engineering
South China University of Technology
Guangzhou 510640, China

ABSTRACT

A multiscale modeling that integrates electronic scale *ab initio* quantum mechanical calculation, atomic scale molecular dynamics simulation, and continuum scale two-temperature model description of the femtosecond laser processing of nickel film at different thicknesses is carried out in this paper. The electron thermophysical parameters (heat capacity, thermal conductivity, and electron-phonon coupling factor) are calculated from first principles modeling, which are further substituted into molecular dynamics and two-temperature model coupled energy equations of electrons and phonons. The melting thresholds for nickel films of different thicknesses are determined from multiscale simulation. Excellent agreement between results from simulation and experiment is achieved, which demonstrates the validity of modeled multiscale framework and its promising potential to predict more complicate cases of femtosecond laser material processing. When it comes to process nickel film via femtosecond laser, the quantitatively calculated maximum thermal diffusion length provides helpful information on choosing the film thickness.

KEYWORDS

Femtosecond Laser; Multiscale Modeling; Melting.

INTRODUCTION

In the past decades, femtosecond laser micro-/nano-fabrication has drawn increasingly hot attentions [1–3], which drives accurate and comprehensive modeling and computation of laser material processing. Since the electron-electron scattering rate is much faster than that of electron-phonon scattering rate, the laser energy is firstly absorbed by electron subsystem at timescale of femtosecond [4]. Meanwhile, the lattice still keeps at room temperature. Subsequently, with the progress of electron-phonon interaction, the lattice gradually becomes heated and finally results in thermal melting [5]. According to the energy equation of electron subsystem, the degree of temperature increase is impacted by electron heat capacity C_e, electron thermal conductivity k_e and electron-phonon coupling factor G_{e-ph} [6–8]. At the atomic scale, thermal response of atomic arrangement and motion to incident laser energy, contain rich information on mechanism of phase change from solid to liquid [9]. Moreover, the propagation of thermal stress can also be detected from atomic interaction [10,11].

As for the response of electron thermophysical properties upon ultrashort laser excitation, *ab initio* quantum mechanical (QM) calculation of electron-phonon coupling and electron heat capacity for representative metals under was performed by Lin *et al.* [12]. Nevertheless, the effect of electron density of states

g change at different electron temperature T_e was not taken into account. By means of density functional theory, the electronic properties of various metals were investigated by Bévillon *et al.* [13]. The strong adjustments of electronic structures of transition metals having partially filled d-bands, such as nickel, copper, silver and platinum, were found. The phenomenological electron-phonon coupling was derived by Chen *et al.* [14], which exhibited excellent agreement with the experimental ablation depth for gold film.

Besides modeling the electronic response to ultrafast high-energy excitation, molecular dynamics (MD) simulation was extensively used to study laser material processing. MD simulation is a powerful tool to study thermal and mechanical behavior of atoms upon femtosecond laser irradiation. The scenarios from femtosecond laser melting [10,11], ablation [9,15], spallation [16–18] were seen. The two-temperature model (TTM) [19], its quantum treatment [20] and semi-classical approximation [21] were developed. Combining with MD simulation at atomic scale and TTM at continuum scale, the numerical calculation results show advantages of both MD and TTM [22–27]. Moreover, an QM, MD and TTM integrated framework was established to illustrate the importance of modeling C_e [6], k_e [7] and G_{e-ph} [8] in our recent work. The program of QM, MD and TTM integrated multiscale framework employed in this paper was developed as extensions on the basis of ABINIT [28] and IMD [29], which are two open-source packages distributed under the GNU General Public License. Nevertheless, a quantitative assessment and comparison with the experimental results and those from the multiscale framework are still absent.

In this paper, an QM-MD-TTM integrated multiscale framework is to be implemented to study thickness dependent melting threshold for femtosecond laser heating nickel film.

NOMENCLATURE

A	Constant, $s^{-1}K^{-2}$
B	Constant, $s^{-1}K^{-1}$
C	Heat capacity, $J/(m^3K)$
D	Diffusion rate, m^2/s
ε	Energy, eV
E	Energy, J
f	Repetition rate, MHz
g	Electron density of states per atom
G	Electron-phonon coupling factor, $W/(m^3K)$
$\hbar$	Reduced Planck constant, eVs
i	Integer number
I	Laser intensity, W/m^2
j	Integer number
J	Laser fluence, J/m^2
k	Thermal conductivity, $W/(mK)$
k_B	Boltzmann constant, J/K
$\lambda\langle\omega^2\rangle$	Second momentum of spectral function, meV^2
L	Length, m
m	Mass, kg
N	Integer number
r	Position, m
R	Radius, m
S	Laser intensity, W/m^3
σ	Standard deviation of Guassian laser profile, s
τ	Relaxation time, s
t	Time, s
T	Temperature, K
υ	Scattering rate, $1/s$
v	Velocity, m/s
V	Volume, m^3
$\lambda\langle\omega^2\rangle$	Second momentum of spectral function, meV^2
x	Direction
y	Direction
z	Direction

MODELING AND SIMULATION

A brief recall of the multiscale framework is presented as follows. More detailed derivation process for each scale can be found elsewhere [10]. As aforementioned, femtosecond laser energy will be absorbed by electron subsystem firstly, once a femtosecond laser pulse irradiates on the surface of metal film. The evolution of temporarily deposited laser energy in electron subsystem follows the energy equation

$$C_e\frac{\partial T_e}{\partial t} = \nabla(k_e\nabla T_e) - G_{e-ph}(T_e - T_l) + S \tag{1}$$

The femtosecond laser energy source term S in Eq. (1) is

$$S(x,t) = \frac{I_{Max}(1-R)}{L_{op}} exp\left(-\frac{x}{L_{op}}\right) exp\left[-\frac{(t-t_0)^2}{2\sigma^2}\right] \tag{2}$$

where I_{max} is the maximum laser intensity, R is the reflectivity of material to incident laser pulse, L_{op} is the laser optical penetration depth, σ is the standard deviation of Guassian profile. The laser pulse duration t_p equals $2\sqrt{2ln2}\sigma$, which represents the full width at half maximum I_{Max} at the temporal point $t_p + t_0$. Hence, the absorbed laser fluence is derived as $\sqrt{\pi ln2}/2t_pI_{Max}$.

At given T_e, electron heat capacity C_e, electron thermal conductivity k_e and electron-phonon coupling factor G_{e-ph} are modeled and computed from QM calculation [6–8]

$$\begin{cases} C_e|_{T_e} = \frac{1}{V_c}\int_{-\infty}^{\infty}\left(\frac{\partial g|_{T_e}}{\partial T_e}f|_{T_e} + g|_{T_e}\frac{\partial f|_{T_e}}{\partial T_e}\right)\varepsilon d\varepsilon \\ k_e|_{T_e} = \frac{1}{3V_c}v_F^2\tau_e|_{T_e}\int_{-\infty}^{\infty}(\frac{\partial g|_{T_e}}{\partial T_e}f|_{T_e} + g|_{T_e}\frac{\partial f|_{T_e}}{\partial T_e})\varepsilon d\varepsilon \\ G_{e-ph}|_{T_e} = \frac{1}{V_c}\frac{\pi\hbar k_B\lambda\langle\omega^2\rangle|_{T_e}}{g_{\varepsilon_F}|_{T_e}}\int_{-\infty}^{\infty}g|_{T_e}^2(-\frac{\partial f|_{T_e}}{\partial\varepsilon})d\varepsilon \end{cases} \tag{3}$$

By calculating the volume V_c that an atom occupies, the Fermi-Dirac distribution function f, the electron density of states g and the second momentum of electron-phonon spectral function $\lambda\langle\omega^2\rangle$, C_e, k_e and G_{e-ph} at given T_e can be obtained from Eq. (3). According to Mattiessen rule [30], the

electron relaxation time τ_e is equal to reciprocal of summation of electron-electron scattering rate $\upsilon_{e-e} = AT_e^2$ and electron-phonon scattering rate $\upsilon_{e-ph} = BT_l$. More specifically, τ_e equals $1/(AT_e^2 + BT_l)$.

In *ab initio* QM calculation, the normal conserving pseudopotential was implement to describe the complicated effects of motion of core electrons, while the valence electrons of $4s^2 3d^8$ were explicitly included to represent the femtosecond laser excited states. After convergence tests regarding cutoff and k-point grids, a cutoff of $46\ Ha$ and $10 \times 10 \times 10$ Monkhorst-Pack k-point grids were chosen. The finite temperature density functional theory (FT-DFT) was adopted to quantify f, g and $\lambda\langle\omega^2\rangle$ at given T_e.

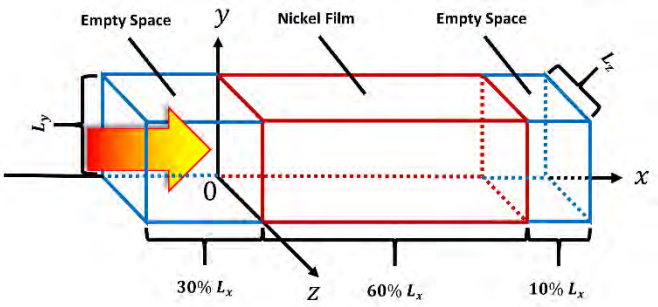

Fig. 1 Schematic diagram of the computational domain. The film thickness L_x varies for different computational cases. The width L_y and height L_z are $3.524\ nm$ and $3.524\ nm$ respectivel . The original surface ($x = 0$) la s on the front surface of nickel film.

Figure 1 schematically illustrates the computational domain. Considering the radius of femtosecond laser pulse is in length scale of several microns, which is much greater than the lateral sizes of computational domain in this paper, the simulation domain was simplified as one-dimensional in the x-direction. Periodic boundary conditions were imposed in the y- and z-directions. Free boundary conditions were set for the front and rear surfaces of nickel film.

The MD simulation is coupled with TTM in Eq. (1) by running a time step Δt_{MD}, N_t times of finite difference method (FDM) computations are performed with a time step Δt_{FDM}. The computational domain is equally divided into N_{FDM} cells with volume of V_{FDM} in the x-direction and N_{Atom} atoms contained in one cell. Based on the temporal evolution of simulation, N_{Atom} varies with the number of atoms in a fixed cell. The electron-phonon coupled thermal energy transfer during Δt_{MD} is

$$E_{e-ph} = \frac{\Delta t_{MD}}{n_t} \sum_{j=1}^{N_t} G_{e-ph} V_{FDM} (T_e^j - T_l) \qquad (4)$$

where T_e^j is the average electron temperature during Δt_{MD}. An additional force acts on nuclei as a result of electron-phonon coupled thermal energy transfer. Therefore, the equation of motion for atom i in MD simulation becomes

$$m_i \frac{d^2 \boldsymbol{r_i}}{dt^2} = -\nabla U + \frac{E_{e-ph}}{\Delta t_{MD}} \frac{m_i v_i^T}{\sum_{k=1}^{N_{Atom}} m_k (v_k^T)^2} \qquad (5)$$

where m_i, r_i and v_i^T are the mass, position and thermal velocity of atom i. By fitting the potential energy surface from QM calculation [31], embedded atom method (EAM) was utilized to describe the interatomic potential U of nickel atoms.

The entire simulation was divided into three stages. As the first step, the modeled system was prepared in terms of NVT ensemble (constant number of atoms, constant volume and constant temperature) to create thermal equilibrium at $300\ K$, which ran for $5\ ps$. Subsequently, the temperature control of Nosé-Hoover thermostat [32] was released to let the system run as NVE ensemble (constant number of atoms, constant volume and constant energy), which also ran for $5\ ps$. The femtosecond laser irradiation started at the third stage, which ran for $90\ ps$ to ensure the melting behavior of laser heated surface can been detected. Table 1 lists the detailed parameters describing the multiscale simulation.

Table 1 Parameters describing the multiscale simulation

Parameter	Value
$A\ (s^{-1}K^{-2})$	1.4×10^6 [26]
$B\ (s^{-1}K^{-1})$	1.624×10^{13} [26]
$L_{op}\ (nm)$	10.5 [33]
N_t	100
$t_0\ (ps)$	20
$t_p\ (fs)$	200
$\Delta t_{FDM}\ (fs)$	0.01
$\Delta t_{MD}\ (fs)$	1
$v_F\ (m/s)$	1.78×10^6 [34]
$V_{FDM}\ (nm^3)$	8.21

RESULTS AND DISCUSSION

Electron Thermoph sical Responses to Laser Irradiation.

The QM quantified distributions of g and f at given T_e are shown in Fig. 2. As seen in the inset of Fig. 2(a), a minor left shift of g to lower ε appears at elevated T_e. Combining with Eq. (3), it can be concluded the left shift of g brings negative impacts on C_e, k_e and G_{e-ph}. Moreover, the Fermi smearing is obvious in Fig. 2(b). Due to the increase of chemical potential at elevated T_e, f shifts to higher ε, which can be seen from the point of ε when $f = 0.5$. The QM calculated g_{ε_F} and $\lambda\langle\omega^2\rangle$ are plotted in Fig. 3. Both g_{ε_F} and $\lambda\langle\omega^2\rangle$ monotonically decrease with the increase of T_e. Recalling the third equation in the groups of Eq. (3), the decrease of g_{ε_F} causes inverse increasing effect of G_{e-ph}. However, the decrease of $\lambda\langle\omega^2\rangle$ brings decreasing G_{e-ph}. Since the percentage of decrement for $\lambda\langle\omega^2\rangle$ is much greater than that for g_{ε_F}, the overall variations of g_{ε_F} and $\lambda\langle\omega^2\rangle$ put negative effects on G_{e-ph} at elevated T_e.

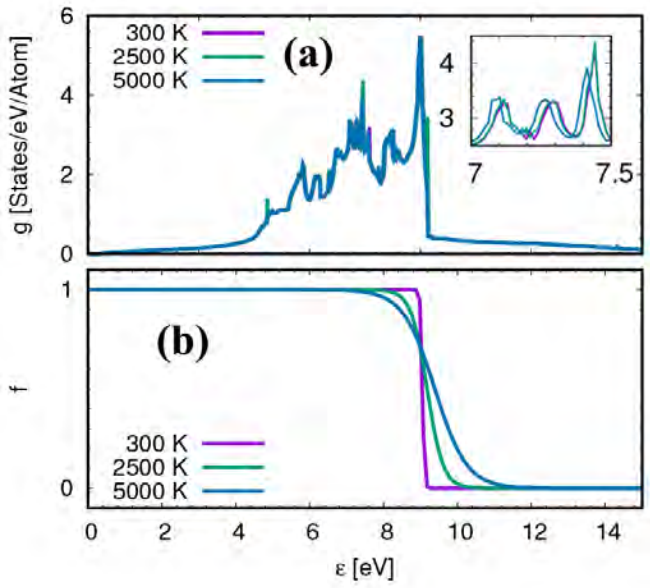

Fig. 2 (a) Electron densit of states g and (b) Fermi-Dirac function f at given electron temperature T_e.

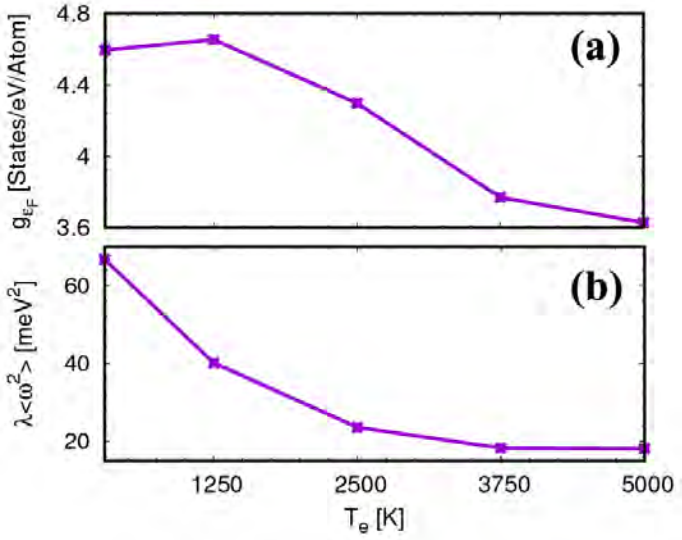

Fig. 3 (a) Electron densit of states g at Fermi energ and (b) the second momentum of electron-phonon spectral function $\lambda\langle\omega^2\rangle$ with the increase of electron temperature T_e.

After obtaining the data of f, g and $\lambda\langle\omega^2\rangle$ in Figs. 2 and 3, C_e, k_e and G_{e-ph} are calculated. For the purpose of comparison, C_e estimated from the experimental result [35] and the one does not consider variation of g in Eq. (2) at increased T_e [12] are plotted together. Since the variation of g is extremely small with at elevated T_e, C_e in the present work and that obtained from T_e independent g almost overlap. However, the experimental result deviates greatly when $T_e > 500\ K$.

As seen in Fig. 4(b), both T_e and T_l influence k_e. With the increase of T_e, k_e presents increasing profile. At different T_l,

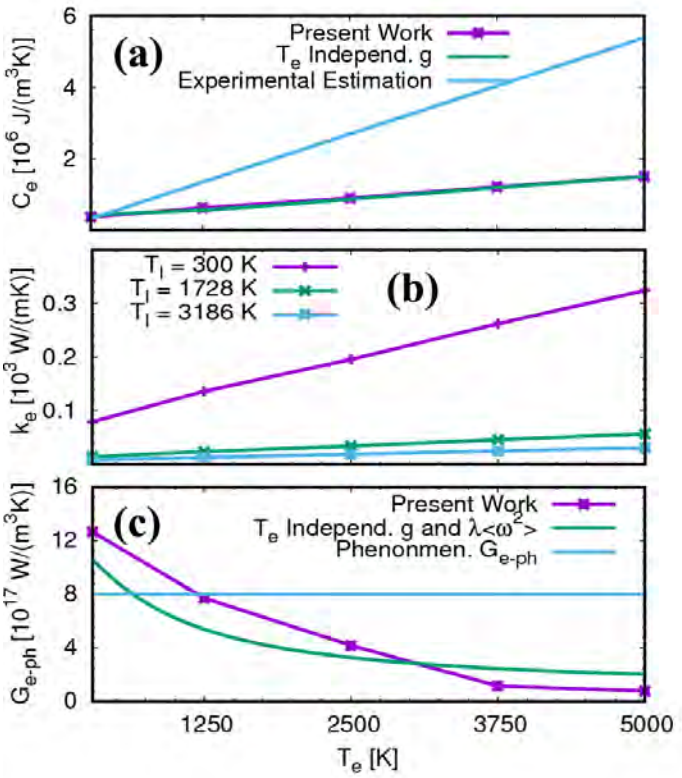

Fig. 4 *Ab initio* quantum mechanical calculation results of distributions of (a) electron heat capacit C_e (b) electron thermal conductivit k_e and (c) electron-phonon coupling factor with the increase of electron temperature T_e.

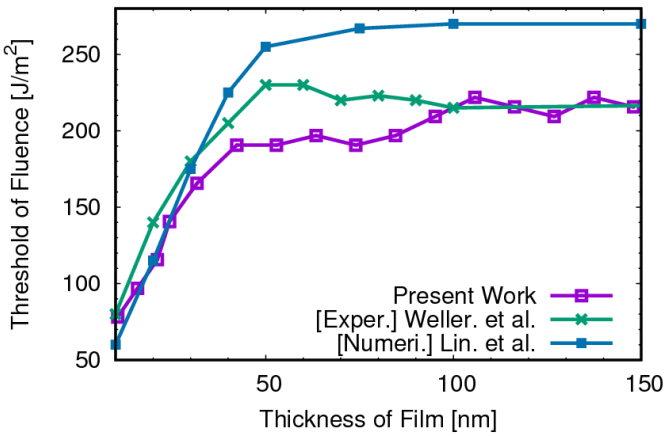

Fig. 5 Thickness dependent melting thresholds of nickel film.

the three cases with T_l at room temperature $300K$, melting point $1728\ K$ and boiling point $3186\ K$ are plotted in Fig. 4(b). For the three cases at the same T_e, higher T_l results in lower k_e. The greatly decreased k_e at high T_l inhibits the temporally deposited laser energy in electron subsystem conducting to deeper region, which makes the majority of high energy in electron subsystem transporting out via electron-phonon coupled heat transfer, rather than electron heat

conduction. In other words, the low k_e at high T_l aggravates the localized femtosecond laser heating and finally leads to the limited volume of melting pool.

In Fig. 4(c), the decrease of G_{e-ph} calculated in this paper is in accord with the decrease $\lambda\langle\omega^2\rangle$ in Fig. 3(b), which verifies that $\lambda\langle\omega^2\rangle$ is dominant in determining G_{e-ph} with the increase of T_e. For the case ignoring variation of g and $\lambda\langle\omega^2\rangle$ at increased T_e [12], the lower G_{e-ph} in [12] than G_{e-ph} calculated in this paper is because the empirical estimation of $\lambda\langle\omega^2\rangle = 49.5\ meV^2$ from experimental result is lower than $\lambda\langle\omega^2\rangle = 66.72\ meV^2$ at room temperature. For the case deriving G_{e-ph} from the phenomenological model [14], no appreciable T_e dependence is observed in Fig. 4(c).

Thickness Dependent Melting Thresholds of Nickel Film.

By setting the same femtosecond laser parameters with those in experimental work [36] and TTM numerical calculation with partial electron thermophysical parameters obtained from QM method [37], the determination of thickness dependent melting thresholds of nickel film was carried out in this paper. According to [37], the melting threshold was defined as the laser fluence induced surface lattice temperature reaches the melting point $1728\ K$ of nickel. For the purpose of comparison, results from [36,37] and the one from present work are shown in Fig. 5. With the increase of film thickness from $10\ nm$ to $45\ nm$, the melting threshold presents linear increasing for all the three results. After $45\ nm$, the melting threshold gradually gets developed, which indicates the influence of film thickness to the melting threshold becomes weak. At the thickness of $10\ nm$, an excellent agreement is seen between the threshold from present work and that from experimental measurement. However, with the increase of thickness from $20\ nm$ to $30\ nm$, another agreement between melting threshold from the present QM-MD-TTM integrated simulation and that from TTM calculation is seen. As the threshold fully developed after $100\ nm$, the results in this paper show better agreement with the experimental results than those from TTM calculation.

In order to find the mechanism leading to different forms of developing and developed threshold profiles, the temporal and spatial evolutions of electron temperature T_e and lattice temperature T_l were calculated. The results shown in Figs. 6 and 7 are for the cases with thicknesses of $31.72\ nm$ and $137.44\ nm$. The corresponding laser fluences for the two cases are melting thresholds, $168.75\ J/m^2$ and $218.75\ J/m^2$, respectively.

As seen in Figs. 6(a) and 7(a), the electron subsystem is thoroughly heated for the $31.72\ nm$ nickel film, while a limited heating depth of $45\ nm$ for the electron subsystem is observed for the $137.44\ nm$ nickel film. Recalling the definition of the maximum thermal diffusion length of femtosecond laser excited electron $L_{Max} = \sqrt{\pi D_e \tau_{Equ}}$ [36], the T_e dependent L_{Max} was calculated in Fig. 8. Meanwhile, Fig. 8 also shows the time τ_{Equ} needed for hot electron subsystem and cold lattice subsystem to reach equilibrium sate, which is estimated from the ratio of C_e to G_{e-ph}. As seen in Fig. 8, τ_{Equ} is in time scale of picoseconds, which agrees with the time needed for electron and lattice get equilibrium in Figs. 6 and 7.

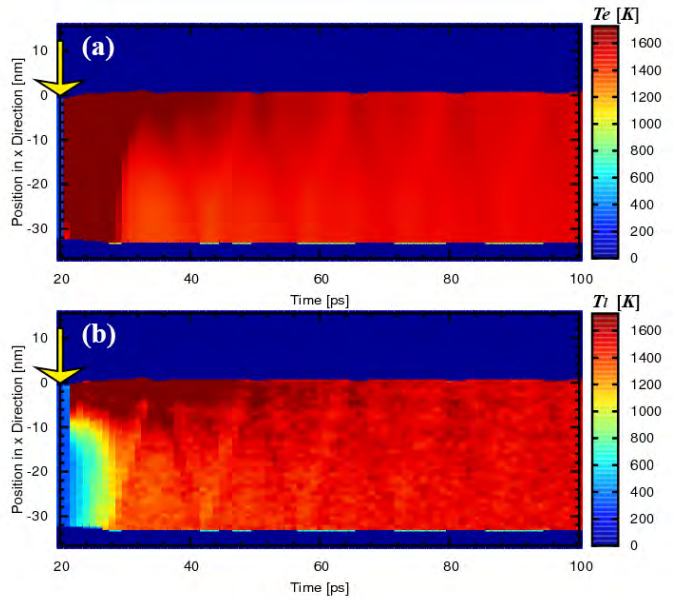

Fig. 6 Temporal and spatial evolutions of electron temperature T_e and lattice temperature T_l with the melting threshold fluence $J_{abs} = 168.75\ J/m^2$ irradiating on a nickel film with thickness of $31.72\ nm$. The ellow arrow denotes femtosecond laser irradiation happens at $x = 0\ nm$ and $t_0 = 20\ ps$.

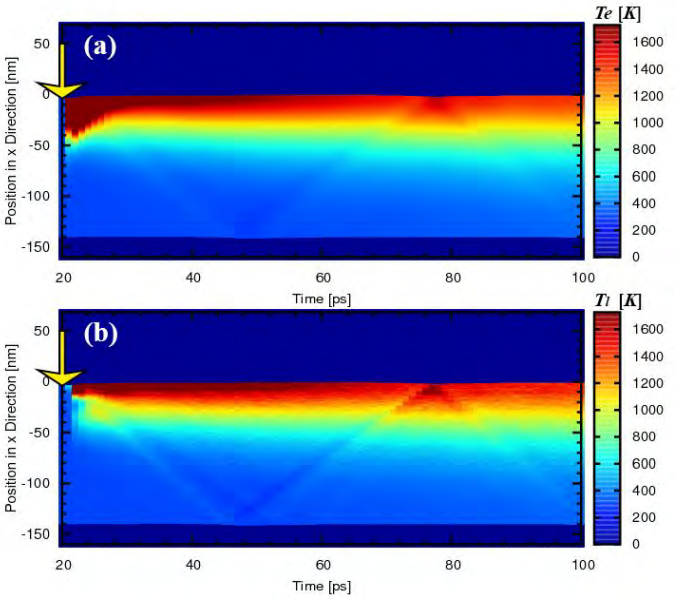

Fig. 7 Temporal and spatial evolutions of electron temperature T_e and lattice temperature T_l with the melting threshold fluence $J_{abs} = 218.75\ J/m^2$ irradiating on a nickel film with thickness of $137.44\ nm$. The ellow arrow denotes femtosecond laser irradiation happens at $x = 0\ nm$ and $t_0 = 20\ ps$.

An alternative interpretation of τ_{Equ} is the time required for certain amount of laser energy C_e with a volume of $1\ m^3$ to transport from the electron subsystem to the lattice subsystem [38]. For all the cases performed in this paper, as checked from the spatial distribution of T_e, its maximum value is $\sim 5000\ K$. The calculated L_{Max} in Fig. 8 at $5000\ K$ is $59\ nm$. By taking the fast cooling of electron subsystem into account, the observed L_{Max} equals $45\ nm$ is reasonable. Meanwhile, the electron-phonon coupled heat transfer further induces lattice subsystem heating in Figs. 6(b) and 7(b). Even though J_{abs} for the case in Fig. 6(a) is smaller, the overall degree of laser heating for the $31.72\ nm$ nickel film is much higher than that for the $137.44\ nm$ nickel film. The main reason comes from L_{Max} is greater than $31.72\ nm$.

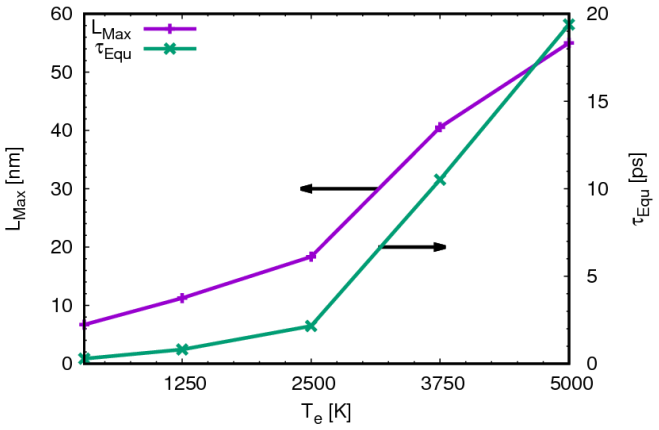

Fig. 8 ***Ab initio*** **quantum mechanical calculation results of the maximum thermal diffusion length L_{max} and the electron-phonon relaxation time τ_{Equ}.**

CONCLUSIONS

Femtosecond laser heating of nickel film is investigated under the framework of quantum mechanics, molecular dynamics and two-temperature model integrated modeling. By performing a serials of cases with nickel film thickness ranging from $10.57\ nm$ to $148.01\ nm$, the film thickness dependent melting threshold is quantified. The transition from linear increase of melting threshold to developed melting threshold is because of the maximum thermal diffusion length. Better agreement with the experimental results than those calculated from the two-temperature model is obtained, which proves it is essential to include the femtosecond laser excitation of electron density of state, the Fermi-Dirac distribution and the second momentum of electron-phonon spectral function in multiscale modeling. Meanwhile, when it comes to process nickel film via femtosecond laser, the quantitatively calculated maximum thermal diffusion length provides helpful information on choosing the film thickness.

ACKNOWLEDGMENTS

Support for this work by the National Natural Science Foundation of China under grant numbers 51705234, U1537202 and 2015B010132005, the Shenzhen Key Laboratory for Additive Manufacturing of High-performance Materials under grant number ZDSYS201703031748354, the Southern University of Science and Technology Presidential Postdoctoral Fellowship and the projected funded by China Postdoctoral Science Foundation under grant number 2017M612653 are gratefully acknowledged.

REFERENCES

[1] Cahill, D. G., Ford, W. K., Goodson, K. E., Mahan, G. D., Majumdar, A., Maris, H. J., Merlin, R., and Phillpot, S. R., 2003, "Nanoscale Thermal Transport," J. Appl. Phys., **93**(2), p. 793.

[2] Cahill, D. G., Braun, P. V., Chen, G., Clarke, D. R., Fan, S., Goodson, K. E., Keblinski, P., King, W. P., Mahan, G. D., Majumdar, A., Maris, H. J., Phillpot, S. R., Pop, E., and Shi, L., 2014, "Nanoscale Thermal Transport. II. 2003–2012," Appl. Phys. Rev., **1**(1), p. 011305.

[3] Jiang, L., Wang, A.-D., Li, B., Cui, T.-H., and Lu, Y.-F., 2018, "Electrons Dynamics Control by Shaping Femtosecond Laser Pulses in Micro/Nanofabrication: Modeling, Method, Measurement and Application," Light Sci. Appl., **7**(2), p. 17134.

[4] Ji, P., and Zhang, Y., 2013, "Femtosecond Laser Processing of Germanium: An Ab Initio Molecular Dynamics Study," J. Phys. D. Appl. Phys., **46**, p. 495108.

[5] Tzou, D. Y., 1995, "A Unified Field Approach for Heat Conduction From Macro- to Micro-Scales," J. Heat Transfer, **117**(1), pp. 8–16.

[6] Ji, P., and Zhang, Y., 2016, "Continuum-Atomistic Simulation of Picosecond Laser Heating of Copper with Electron Heat Capacity from Ab Initio Calculation," Chem. Phys. Lett., **648**, pp. 109–113.

[7] Ji, P., and Zhang, Y., 2017, "Multiscale Modeling of Femtosecond Laser Irradiation on Copper Film with Electron Thermal Conductivity from Ab Initio Calculation," Numer. Heat Transf. Part A Appl., **71**(2), pp. 128–136.

[8] Ji, P., and Zhang, Y., 2016, "Ab Initio Determination of Effective Electron–phonon Coupling Factor in Copper," Phys. Lett. A, **380**(17), pp. 1551–1555.

[9] Li, X., Jiang, L., and Tsai, H.-L., 2009, "Phase Change Mechanisms during Femtosecond Laser Pulse Train Ablation of Nickel Thin Films," J. Appl. Phys., **106**(6), p. 064906.

[10] Ji, P., and Zhang, Y., 2017, "Melting and Thermal Ablation of a Silver Film Induced by Femtosecond Laser Heating: A Multiscale Modeling Approach," Appl. Phys. A, **123**(10), p. 671.

[11] Gan, Y., and Chen, J. K., 2010, "Thermomechanical Wave Propagation in Gold Films Induced by Ultrashort Laser Pulses," Mech. Mater., **42**(4), pp. 491–501.

[12] Lin, Z., Zhigilei, L. V., and Celli, V., 2008, "Electron-Phonon Coupling and Electron Heat Capacity of Metals under Conditions of Strong Electron-Phonon Nonequilibrium," Phys. Rev. B, **77**(7), p. 075133.

[13] Bévillon, E., Colombier, J. P., Recoules, V., and Stoian,

R., 2014, “Free-Electron Properties of Metals under Ultrafast Laser-Induced Electron-Phonon Nonequilibrium: A First-Principles Study,” Phys. Rev. B, **89**(11), p. 115117.

[14] J. K. Chen, W. P. Latham, and J. E. Beraun, 2005, “The Role of Electron–phonon Coupling in Ultrafast Laser Heating,” J. Laser Appl., **17**(1), p. 63.

[15] Sonntag, S., Paredes, C. T., Roth, J., and Trebin, H. R., 2011, “Molecular Dynamics Simulations of Cluster Distribution from Femtosecond Laser Ablation in Aluminum,” Appl. Phys. A Mater. Sci. Process., **104**(2), pp. 559–565.

[16] Leveugle, E., Ivanov, D. S., and Zhigilei, L. V., 2004, “Photomechanical Spallation of Molecular and Metal Targets: Molecular Dynamics Study,” Appl. Phys. A Mater. Sci. Process., **79**(7), pp. 1643–1655.

[17] Demaske, B. J., Zhakhovsky, V. V., Inogamov, N. A., and Oleynik, I. I., 2010, “Ablation and Spallation of Gold Films Irradiated by Ultrashort Laser Pulses,” Phys. Rev. B, **82**(6), pp. 1–5.

[18] Wu, C., and Zhigilei, L. V, 2014, “Microscopic Mechanisms of Laser Spallation and Ablation of Metal Targets from Large-Scale Molecular Dynamics Simulations,” Appl. Phys. A, **114**(1), pp. 11–32.

[19] Allen, P. B., and Dynes, R. C., 1975, “Transition Temperature of Strong-Couple Superconductors Reanalyzed,” Phys. Rev. B, **12**(3), pp. 905–922.

[20] Jiang, L., and Tsai, H.-L., 2005, “Improved Two-Temperature Model and Its Application in Ultrashort Laser Heating of Metal Films,” J. Heat Transfer, **127**(10), p. 1167.

[21] Chen, J. K., Tzou, D. Y., and Beraun, J. E., 2006, “A Semiclassical Two-Temperature Model for Ultrafast Laser Heating,” Int. J. Heat Mass Transf., **49**(1–2), pp. 307–316.

[22] Gan, Y., Wang, C., and Chen, Z., 2015, “Ultrafast Laser-Excited Vibration and Elastic Modulus of Individual Gold Nanorods,” Opt. Lett., **40**(3), pp. 340–343.

[23] Roth, J., Trebin, H. R., Kiselev, A., and Rapp, D. M., 2016, “Laser Ablation of Al–Ni Alloys and Multilayers,” Appl. Phys. A Mater. Sci. Process., **122**(5), p. 500.

[24] Zhigilei, L. V. L., Lin, Z., and Ivanov, D. S. D., 2009, “Atomistic Modeling of Short Pulse Laser Ablation of Metals: Connections between Melting, Spallation, and Phase Explosion†,” J. Phys. Chem. C, **113**(27), pp. 11892–11906.

[25] Holst, B., Recoules, V., Mazevet, S., Torrent, M., Ng, A., Chen, Z., Kirkwood, S. E., Sametoglu, V., Reid, M., and Tsui, Y. Y., 2014, “Ab Initio Model of Optical Properties of Two-Temperature Warm Dense Matter,” Phys. Rev. B, **90**(3), p. 035121.

[26] Ivanov, D. S., and Zhigilei, L. V., 2003, “Combined Atomistic-Continuum Modeling of Short-Pulse Laser Melting and Disintegration of Metal Films,” Phys. Rev. B, **68**(6), p. 064114.

[27] Xiong, Q. L., Tian, X. G., and Lu, T. J., 2012, “Atomistic Modeling of Electron Relaxation Effect on Femtosecond Laser-Induced Thermoelastic Response of Gold Films,” J. Appl. Phys., **112**(2), p. 024313.

[28] Gonze, X., Amadon, B., Anglade, P.-M., Beuken, J.-M., Bottin, F., Boulanger, P., Bruneval, F., Caliste, D., Caracas, R., Côté, M., Deutsch, T., Genovese, L., Ghosez, P., Giantomassi, M., Goedecker, S., Hamann, D. R. R., Hermet, P., Jollet, F., Jomard, G., Leroux, S., Mancini, M., Mazevet, S., Oliveira, M. J. T. J. T., Onida, G., Pouillon, Y., Rangel, T., Rignanese, G.-M., Sangalli, D., Shaltaf, R., Torrent, M., Verstraete, M. J. J., Zerah, G., and Zwanziger, J. W. W., 2009, “ABINIT: First-Principles Approach to Material and Nanosystem Properties,” Comput. Phys. Commun., **180**(12), pp. 2582–2615.

[29] Stadler, J., Mikulla, R., and Trebin, H., 1997, “IMD: A Software Package for Molecular Dynamics Studies on Parallel Computers,” Int. J. Mod. Phys. C, **8**(5), pp. 1131–1140.

[30] Güdde, J., Hohlfeld, J., Müller, J. G., and Matthias, E., 1998, “Damage Threshold Dependence on Electron–phonon Coupling in Au and Ni Films,” Appl. Surf. Sci., **127**–**129**, pp. 40–45.

[31] Sheng, H. W., Kramer, M. J., Cadien, A., Fujita, T., and Chen, M. W., 2011, “Highly Optimized Embedded-Atom-Method Potentials for Fourteen FCC Metals,” Phys. Rev. B, **83**(13), p. 134118.

[32] Ji, P., Zhang, Y., and Yang, M., 2013, “Structural, Dynamic, and Vibrational Properties during Heat Transfer in Si/Ge Superlattices: A Car-Parrinello Molecular Dynamics Study,” J. Appl. Phys., **114**(23), p. 234905.

[33] May, O. C., 1974, “Optical Absorption Coefficient of Nickel, Palladium Platinum and Copper, Silver, Gold between 20 and 120 EV,” Opt. Commun., **11**(1), pp. 62–63.

[34] Ashcroft, N. W., and Mermin, N. D., 1976, *Solid State Physics*, Holt, Rinehart and Winston, New York.

[35] 1972, *American Institute of Physics Handbook*, McGraw-Hill, New York.

[36] Wellershoff, S. S., Gudde, J., Hohlfeld, J., Muller, J. G., and Matthias, E., 1998, “Role of Electron-Phonon Coupling in Femtosecond Laser Damage of Metals,” *Spie*, pp. 378–387.

[37] Lin, Z., and Zhigilei, L. V., 2007, “Temperature Dependences of the Electron-Phonon Coupling, Electron Heat Capacity and Thermal Conductivity in Ni under Femtosecond Laser Irradiation,” Appl. Surf. Sci., **253**(15), pp. 6295–6300.

[38] Ji, P., and Zhang, Y., 2017, “Electron–Phonon Coupled Heat Transfer and Thermal Response Induced by Femtosecond Laser Heating of Gold,” J. Heat Transfer, **139**(5), pp. 52001–52006.